RADARGRAMMETRIC EXPERIMENTS WITH SPACE SHUTTLE SIR-B IMAGERY

F. Leberl [1], G. Domik [1], J. Raggam [2], J. Cimino [3], M. Kobrick [3]

[1] VEXCEL Corporation, Boulder, CO 80301
[2] Graz Research Center, A-8010 Graz, Austria
[3] Jet Propulsion Laboratory, Pasadena, CA 91109

ABSTRACT

SIR-B resulted in the most comprehensive radar image data set for radargrammetric work that is currently available. The paper reviews the results obtained with stereo image pairs and with the creation of secondary radar image products.

1. INTRODUCTION

One of the parameters of great speculation in past radar mapping studies did address the radar look angle and look angle disparities in overlapping stereo images. SIR-B provided a series of radar coverages of radargrammetric interest and with variations of the look angle. In particular data sets were generated as follows:

(a) 3 overlapping strips over Mt. Shasta, California;

(b) 4 overlapping strips over Gordón la Graza, Argentina;

(c) 5 overlapping strips over Josė de San Martin, Argentina;

(d) 3 overlapping strips over Sydney, Australia;

(e) 2 overlapping strips over Illinois.

Analysis of the data began soon after the SIR-B flight in October 1984, first working with the data set (a) of Mt. Shasta. The results have been reported in earlier papers (Leberl et al., 1986a) and Leberl et al. (1986b): the analysis addressed the creation and use of a digital terrain elevation model from the overlapping images.

Of two elaborate data sets from Argentina only one has thus far been analyzed; results for the Gordón la Graza area were reported in papers by Cimino et al. (1986), Domik et al. (1986) and Leberl et al. (1986c).

Finally, very recent and as yet unpublished work provided insights into so-called opposite-side stereo geometry with the help of the Illinois data (e). Data sets (c) and (d) are still awaiting an analysis. Additional radargrammetric work was performed by Ramapryan et al. (1984) emphasizing processing technology. The contributions and experiments of Zebker and Goldstein (1985) to extract topographic relief information through interferometry are not counted into radargrammetric SIR-B work since they employ SAR data in non-image form.

The paper summarizes the parameters for the imaging geometries of the data sets, it describes the current status of SIR-B radargrammetry and presents a discussion of the capabilities and limitations of the data. It will be shown that topographic height measurements can be made with root mean square errors of $\pm$ 10 to 20 m with the data from Illinois, and that precision registration and "geo-coding" is feasible using stereoradargrammetry.

Table 1: Imaging geometries for radargrammetrically processed SIR-B data. Range resolution is 14 m; presentation is with 12.5 m pixels in ground range.

Nr.	Site	Data take	Look angle off-nadir (°)	Ground Resolution (m^2)
1	Mt. Shasta	39.4	57	16 x 34
2	- " -	55.4	51	17 x 29
3	- " -	87.4	28	30 x 21
4	Gordón la Graza	104.4	56	16 x 34
5	- " -	88.4	51	17 x 29
6	- " -	72.4	43	20 x 23
7	- " -	56.4	33	26 x 23
8	Illinois	49.2	28	30 x 21
9	- " -	97.2	29	29 x 21

2. RADAR STEREO MAPPING ACCURACIES

2.1 Theoretical Expectations

Some elementary equations relate the error of point coordinates on the Earth surface to errors of slant range (for example Leberl, 1979):

$$\sigma_{\text{cross-track}} = \sigma_{\text{range}} \cdot (\cos^2 \Theta' + \cos^2 \Theta'')^{1/2} / \sin (\Theta' \pm \Theta'') \quad (1)$$

$$\sigma_{\text{height}} = \sigma_{\text{range}} \cdot (\sin^2 \Theta' + \sin^2 \Theta'')^{1/2} / \sin (\Theta' \pm \Theta'') \quad (2)$$

Equs (1) and (2) result from Figure 1 where Θ', Θ'' is defined as look-angle off-nadir and σ_{range} is the standard error of range. The minus-sign applies to same-side stereo, the plus sign to opposite side.

Another avenue to an error prediction employs parallax differences. These are composed of the two relief displacements p', p" as follows:

$$p = p' \pm p'' = h/\tan \Theta' \pm h/\tan \Theta'' \quad (3)$$

so that

$$\sigma_{\text{height}} = \sigma_p / (\cot \Theta' \pm \cot \Theta'') \quad (4)$$

Equs. (3) and (4) have been used by Koopmans (1974), Derenyi and Stuart (1984) and others. Equations (2) and (4) are directly comparable; equ. (2) applies to a height computation based on the intersection of homologue projection rays (i.e. circles, see Leberl, 1979), whereas equ. (4) is based on height computation with parallax differences. One can relate them to one another by replacing σ_p by

$$\sigma_{p'} = \sigma_{\text{range}} / \sin \Theta' \quad (5)$$

$$\sigma_{p''} = \sigma_{\text{range}} / \sin \Theta''$$

This leads from equ.(4) to

$$\sigma_{\text{height}} = \sigma_{\text{range}} (1/\sin^2 \Theta' + 1/\sin^2 \Theta'')^{1/2} / (\cot \Theta' \pm \cot \Theta'') \quad (6)$$

Seitenzahl/page/pagina

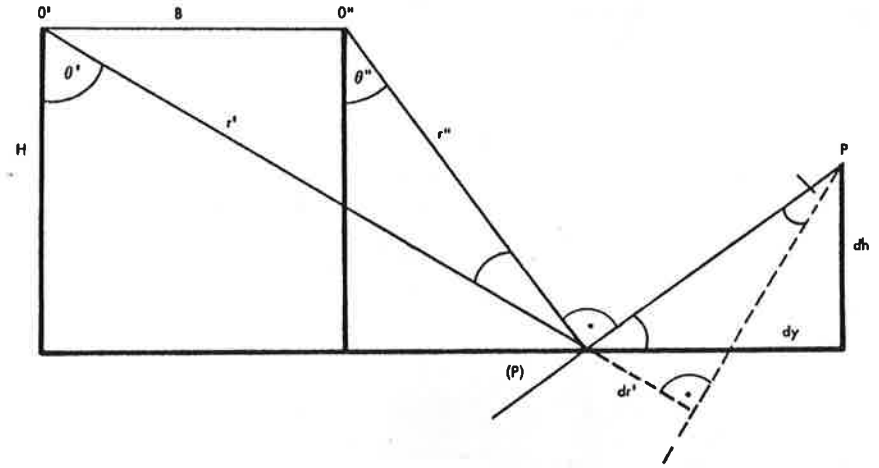

Figure 1: Definition of entities for propagation of range error into errors of height and cross-track coordinates.

Equ. (7) is now easily seen to be identical to equ. (2):

$$\sigma_{height} = \sigma_{range} \cdot ((\sin^2 \theta' + \sin^2 \theta'')^{1/2}/(\sin \theta' \cdot \sin \theta'')).$$
$$.(\sin \theta' \cdot \sin \theta'')/(\sin \theta''.\cos \theta' \pm \sin \theta' \cos \theta'') \qquad (7)$$

Table 2 lists the coefficients of equs. (2) and (4) for the various stereomodels that one can form from the SIR-B data. All stereo-image pairs are from same-side parallel configurations except for the Illinois-case which is opposite side. It is evident that the predicted errors are smaller with larger stereo-intersection angles. Generally the height errors would not be larger than twice the errors of slant range.

The relationship between range resolution and error of slant range is unclear. In the absense of accepted statements on this relationship it is assumed that the standard error of slant range is 1/2 of the range resolution value. This would amount to a σ_{range} of 7 m.

2.2 Accuracy of Model Set-Up and Point Positioning

The work with actual SIR-B images relies on the analytical plotter Kern DSR-11, equipped with the radargrammetric software system SMART that has been discussed by Raggam and Leberl (1984). Image pairs are inserted into the instrument, an image coordinate system is defined and model set-up measurements as well as computations are performed to obtain a parallax-free stereo-model. The computation consists of a so-called "bundle-solution" that relates image coordinates to ground coordinates with the help of ground control points. This is followed by actual data collection of individual points, contour lines and of planimetric detail.

Table 3 summarizes the residual coordinate errors after stereo-model set-up. It is immediately evident that these accuracies are far less than expected from propagation of slant range errors. It was argued in a first discussion of these values in the earlier paper (Leberl et al, 1986b) that this could be caused by poor stereo viewability due to migrating edges such as illustrated in Figures 2 and 3 that show a detail of the Gordón la Graza data. Edge migration in this case is partly caused by the stereo-geometry expressed in parallax differences, and partly by the difference in illumination angles. In featureless rolling terrain such illumination-induced edge migration could be significant. Figure 4 illustrates the concept with the help of a sinusoidal surface relief. At a given position x along the profile, the slope λ is:

$$\tan \lambda = a.b. \cos (b.x) \qquad (8)$$

where a is the amplitude, b the period of the sinusoidal relief.

Seitenzahl/page/pagina

(a)

(b)

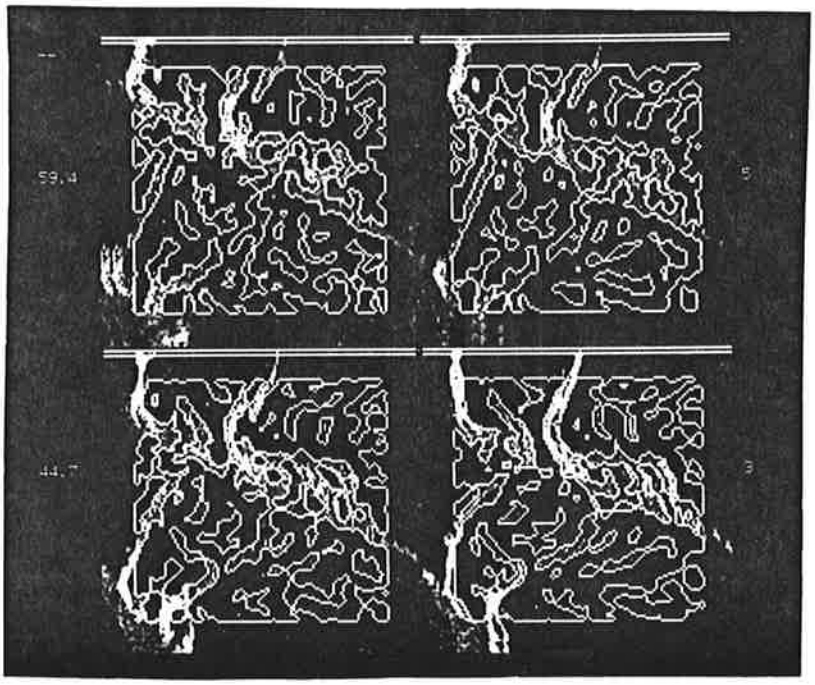

Figure 2: (a) Four image segments of an area in Gordón la Graza, (b) with overlaid edges (Marr-Hildreth zero-crossings).

Table 2: Coefficients for the height errors from SIR-B stereo image pairs.

Stereo pair number	Area	Data takes	$\sigma_{height}/\sigma_{range}$ equ.(2)	$\sigma_{height}/\sigma_{parallax}$ equ.(4)	$\Theta_{cross}/\sigma_{range}$ equ.(1)	Θ'/Θ''	Stereo Intersection (°)
1	Mt.Shasta	39/55	11.1	6.2	8.0	57/51	6
2	"	55/87	2.3	0.9	2.8	51/28	23
3	"	39/87	2.0	0.8	2.2	57/28	28
4	Gordón	104/88	13.0	7.3	9.7	56/51	5
5	"	88/72	7.4	3.8	6.9	51/43	8
6	"	72/56	5.0	2.1	4.9	43/33	10
7	"	104/72	4.8	2.5	4.1	56/43	13
8	"	88/56	3.1	1.4	3.4	51/33	18
9	"	104/56	2.5	1.2	2.6	56/33	23
10	Illinois	49/97	0.80	0.27	1.5	29/28	57

Image brightness I is assumed to be inversely proportional to the incidence angle (Θ-λ), where Θ is the look angle off- nadir:

$$I = c/\sin(\Theta-\lambda) \qquad (9)$$

The local maximum I_{max} of intensity is at the "specular point", located at x_{max}. The local minimum is at the inflection point along the sinus curve, or at the shadow edge.

It is evident from Figure 4 that the specular point will migrate with changes of the look angle off-nadir, with extreme values reached in the opposite-side stereo case. Quantification of the effect will need to be based on further development of equations (8) and (9).

Poor stereo-viewability is certainly a factor of the only processed SIR-B "opposite-side" stereo pair of Illinois. Identification of ground control points indeed is very difficult. Height coordinates, however, are not affected by this limitation. The Illinois data provide a good height accuracy, but display large errors in the XY planimetric coordinates. The edge migration can be expected to be minimal since the terrain is entirely flat, with the exception of small drainage features.

2.3 Stereo-Mapping

The SIR-B stereo-image pairs were used to create experimental topographic map data. Figure 5 is a contour map of the area around Mt. Shasta with a contour interval of 150 m. This contour interval is about 3 times the observed height error, in accordance with cartographic standards.

Seitenzahl/page/pagina

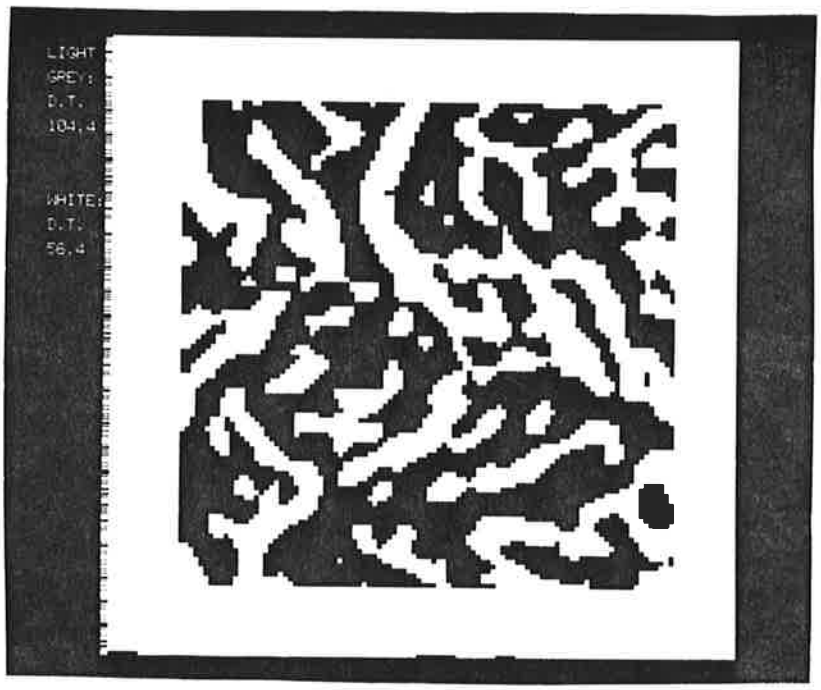

Figure 3: Overlaid pair of "filled" edge images, taken from Fig. 2 b to illustrate the edge migration problem.

Table 3: Residual coordinate errors in meters after stereo-model set-up

Area	Stereomodel Data take	Intersection angle (°)	Coordinate errors in meters North	East	Height
Argentina	104/88	5	67	78	86
	88/72	8	78	70	110
	72/56	10	65	85	67
	104/72	13	77	73	65
	88/56	18	59	74	59
	104/56	23	62	49	62
Mt. Shasta	39/55	6	106	106	125
	55/87	23	44	75	53
	39/87	28	91	100	73
Illinois	49/97	57	240	185	10

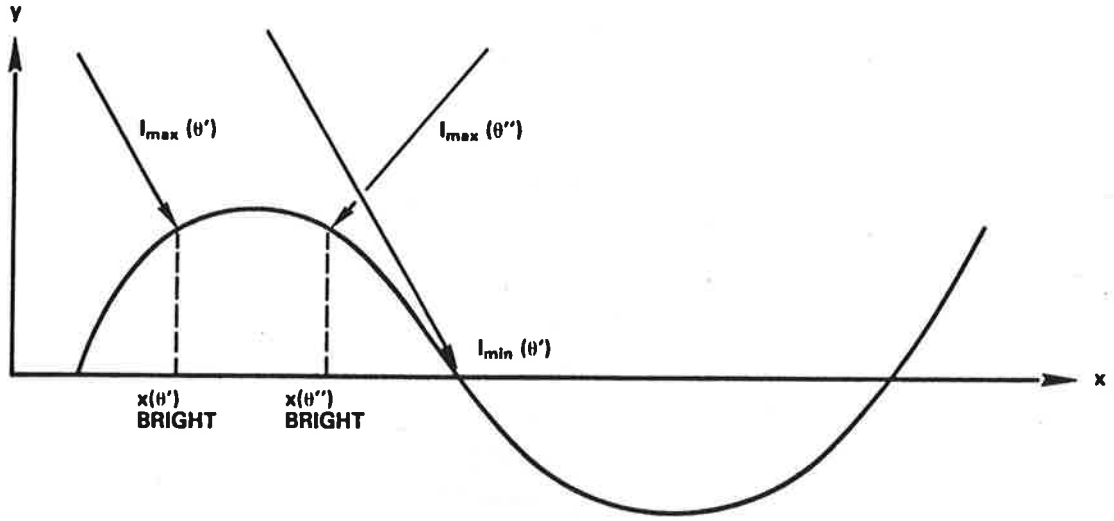

Figure 4: Edge migration as a result of changing look angles.

For Mt. Shasta and for Gordón la Graza, SIR-B image pairs were also the source for digital elevation models. These have been presented at earlier occasions (see reference 8). The use of the radar derived DEMs is for secondary radar images as discussed in the next chapter.

3. SECONDARY RADAR IMAGE PRODUCTS

Domik et al. (1986) illustrate a set of SAR images that are derived from the primary correlator output. Secondary image products are the result of digital image processing. Table 4 lists various types of such products.

Primary interest is of course on the rectified radar image; a new terminology refers to this also as "geo-coded" images. Rectification is achieved using the stereo-derived DEM, and it may concern the geometric resampling of the primary images as well as the radiometric correction for slope effects.

Figure 6 illustrates a set of raw primary images, and their geometric as well as geometrically and radiometrically rectified versions. The application of these and other techniques have been discussed in the papers by Domik et al. (1986) and Cimino et al. (1986). It is evident that rectified multi-date and multi-angle SAR images lend themselves to multi-temporal and incidence-angle-signature analyses.

4. CONCLUSIONS

SIR-B provided for the first time a variety of SAR images at differing look angles that cover areas for stereoscopic analysis. The results lead to the conclusions that

* planimetric and height accuracies are of the same order of magnitude;
* errors are less dependent on intersection angles than previously expected from theoretical predictions;
* the errors are of the order of magnitude of several pixels or range resolution diameters;
* only the steep-looking opposite-side stereo-pair of a flat area (Illinois) produced height accuracies near the theoretical prediction.

Seitenzahl/page/pagina

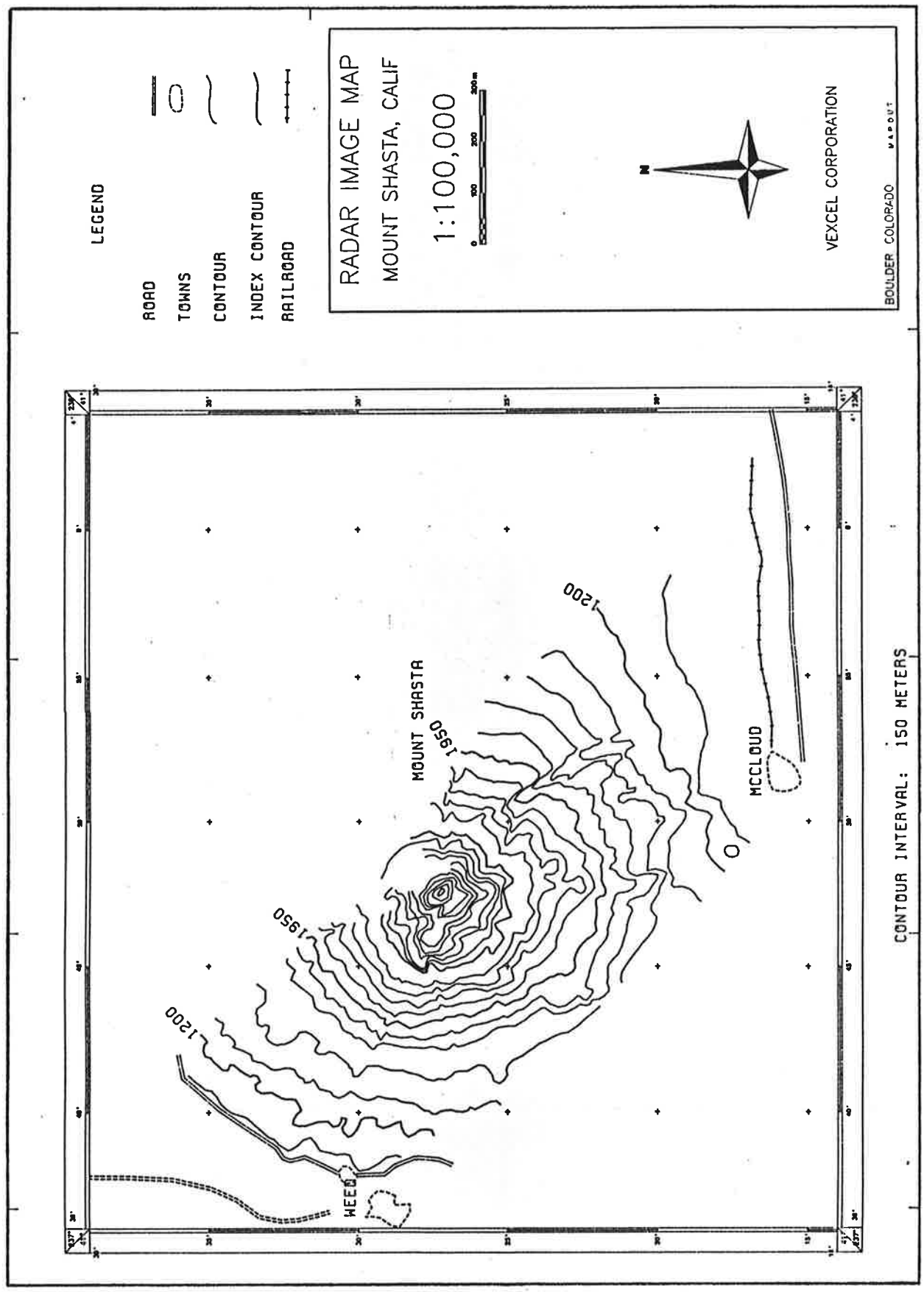

Figure 5: Contour map produced from overlapping pair of SIR-B SAR images of Mt. Shasta (data takes 55.4 and 87.4 at 23° intersection angle).

Figure 6: Raw SIR-B image segment (a), geometric rectification (b) and radiometric rectification (c), of an area in Gordón la Graza, Argentina. The black areas in the radiometrically rectified image are shadows. Coverage is 6.4 x 6.4 sqkms.

(a)

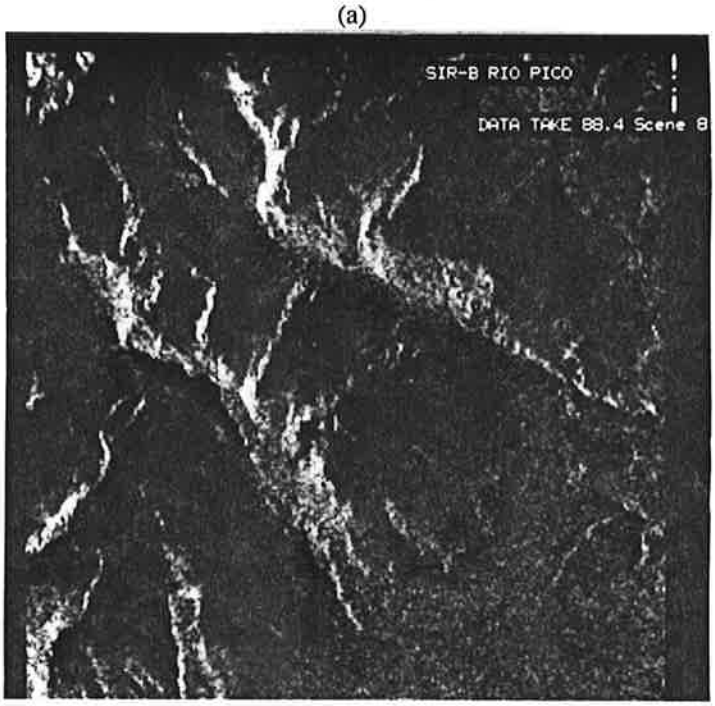

(b)

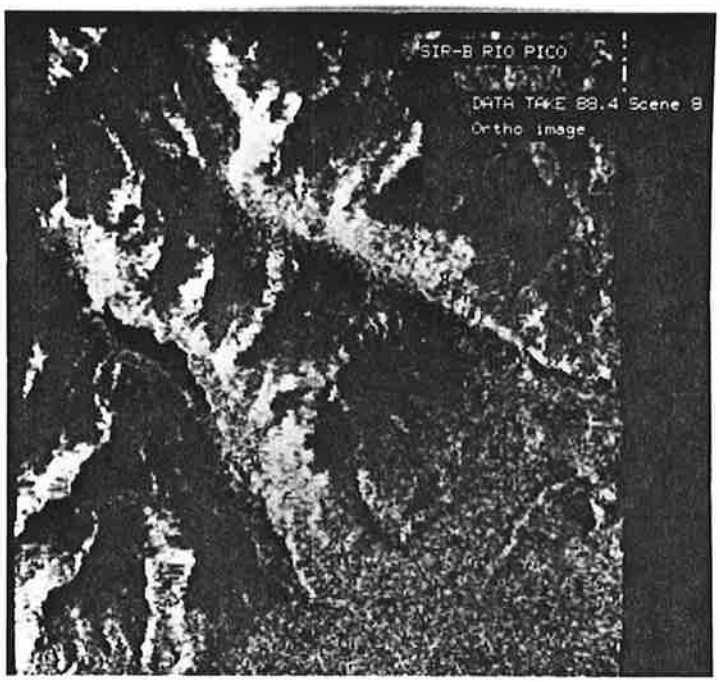

(c)

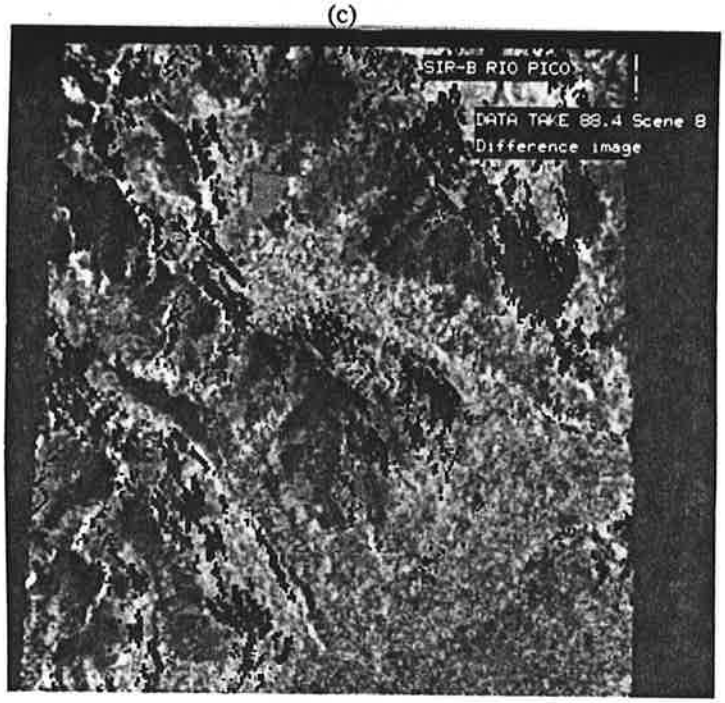

Table 4: Types of secondary radar image products based on multiple radar images and digital elevation models (DEM).

Type of Product	Comment
1. Ortho-Image	Geometrically rectified black and white image to fit a map.
2. False color from multiple ortho images.	Use three geometrically matched ortho- images
3. Simulated radar image	Use of DEM to predict the geometry and radiometry of a radar image, based only on terrain slope and assumed backscatter of surface cover.
4. Radiometrically rectified image	Difference image between simulated and real radar images.
5. False color from multiple radiometrically corrected images.	Use three radiometrically corrected images.
6. Stereo-ortho images from one single image	Create an image pair of which one is geometrically corrected (see 1), the other is the same radar image but has artificially introduced relief-displacement (so-called "stereo-mate").
7. Stereo-ortho images from two source images	As in item 6, but the "stereomate" is produced from a second overlapping radar image.

8.	Composite radar image and DEM	Radar image brightnesses are added to an artificially illuminated DEM to present the relief in conjunction with the radar image.
9.	Topographic radar image map	Composite of an ortho-image, contour lines and planimetric detail (roads, settlements, names, legends, coordinate grid etc.).
10.	Thematic radar image map	Composite of an ortho-image and planimetric detail from a thematic map.
11.	Perspective view of DEM and image density numbers	Same as item 8., but presented as a perspective camera image, to further enhance topographic relief.

Accuracy does not increase in mountainous areas as intersection angles increase. This is suspected to be connected with the increase of edge migration at larger angles of illumination disparity.

The images are at L-band and contain significant speckle noise. This is also a potential cause of accuracy limitations.

The work has resulted in applications for the stereo-derived terrain elevations to rectify the raw images both radiometrically as well as geometrically. This can serve in improved thematic interpretation of single and multiple SAR images, especially if so-called "incidence angle signatures" are the basis for terrain cover discrimination.

Ongoing work will need to further solidify the current numerical results employing additional SIR-B SAR images. It will also have to develop a better understanding of the visual limitations on radar stereo viewing and effects of look-angle induced edge migration.

Acknowledgement

The work was performed in part under contract no. 95743 between VEXCEL Corporation and the Jet Propulsion Laboratory, California Institute of Technology. The Illinois SAR-B opposite-side evaluation was performed under contract no. 95414-x between VEXCEL Corporation and Goodyear Aerospace Corporation, Litchfield Park, Arizona. The participation of Drs. Mike Kobrick and JoBea Cimino was in partial fulfillment of contract NAS7-100 between the Jet Propulsion Laboratory and NASA.

REFERENCES:

Cimino, J., A. Brandani, D. Casey, J. Rabassa, and S. Wall (1986) "Multiple Incidence Angle SIR-B Experiment Over Argentina: Mapping of Vegetation," IEEE Trans. Geoscience, Rem. Sensing, Vol. 24, No. 4.

Derenyi, E., A. Stuart (1984) "Height Determination from Spaceborne Radar Imagery," Proc. ASPRS Ann. Convention, pp. 243-252.

Domik G., F. Leberl, J. Cimino (1986) "Multiple Incidence Angle SIR-B Experiment over Argentina: Generation of Secondary Image Products," IEEE Trans. Geoscience Remote Sensing, Vol. 24, No. 4.

Koopmans, B. (1974) "Drainage Analysis on Radar Images," ITC-Journal 1973-2, Enschede, Netherlands.

Leberl, F. (1979) "Accuracy Aspects of Stereo-Side-Looking Radar," JPL-Publication 1979-17, Jet Propulsion Laboratory, Pasadena, USA.

Leberl, F., G. Domik, J. Raggam, J. Cimino, M. Kobrick (1986a) "Space Shuttle Radargrammetry Results," Proc. of the Ann. Conv. of ASPRS/ACSM, Vol. , pp. 198-201.

Leberl, F., G. Domik, J. Raggam, M. Kobrick (1986b) "Radar Stereomapping Techniques and Application to SIR-B Images of Mt. Shasta," IEEE Trans. Geoscience Remote Sensing, Vol. 24, No. 4.

Leberl, F., G. Domik, J. Raggam, J. Cimino, M. Kobrick (1986c) "Multiple Incidence Angle SIR-B Experiment Over Argentina: Stereo-Radargrammetric Analysis," IEEE Trans. Geoscience Remote Sensing, Vol. 24, No. 4.

Ramapryan, H.K., C.W. Murray, J.P. Strong, H.W. Blodget (1984) "Automated Elevation Mapping and Registration," In "SIR-B Science Investigations Plan," JPL Publ. 84-3, Jet Propulsion Laboratory, Pasadena, CA, pp. 4.118-4.120.

Raggam, J., F. Leberl (1984) "SMART--A Program for Radar Stereo Mapping on the Kern DSR-1," Proceedings, Annual Meeting of the American Society of Photogrammetry, 765-773.

Zebker, H., R. Goldstein (1985) "Topographic Mapping from Interferometric Synthetic Aperture Radar Observations," Proc. IGARSS '85, IEEE Cat. No. 85CH2162-6.